Quaternary Research 84 (2015) 457–466

Contents lists available at ScienceDirect

Quaternary Research

journal homepage: www.elsevier.com/locate/yqres

Late Plio-Pleistocene humidity fluctuations in the western Qaidam Basin (NE Tibetan Plateau) revealed by an integrated magnetic–palynological record from lacustrine sediments

Christian Herb [a], Andreas Koutsodendris [b], Weilin Zhang [a,c], Erwin Appel [a,*], Xiaomin Fang [c], Silke Voigt [d], Jörg Pross [b]

[a] Department of Geosciences, University of Tübingen, Hölderlinstr. 12, 72074 Tübingen, Germany
[b] Paleoenvironmental Dynamics Group, Institute of Earth Sciences, University of Heidelberg, Im Neuenheimer Feld 234, 69120 Heidelberg, Germany
[c] Institute of Tibetan Plateau Research, Chinese Academy of Sciences, Building 3, Courtyard 16, Lin Cui Road, Beijing 100101, China
[d] Institute of Geosciences, University of Frankfurt, Altenhöferallee 1, 60438 Frankfurt, Germany

ARTICLE INFO

Article history:
Received 20 June 2015
Available online 11 November 2015

Keywords:
Magnetic proxies
Pollen
Lacustrine sediments
Paleoclimate
Monsoon
Westerlies
Qaidam Basin
Tibetan Plateau

ABSTRACT

Deciphering the climatic evolution of the Tibetan Plateau region during the Plio-Pleistocene is hampered by the lack of continuous archives and proxy datasets indicative of moisture availability. Here we assess the suitability of magnetic susceptibility (χ) measured on lacustrine sediments as a paleohydrological proxy based on material from drill core SG-1 (2.69–0.08 Ma) from the western Qaidam Basin. Our assessment is based on directly comparing χ with the *Artemisia*/Chenopodiaceae (A/C) pollen ratio, which represents a sensitive, well-established proxy for moisture changes in arid environments. We find that higher and lower χ values represent drier and less dry conditions, respectively, for the Late Plio-Pleistocene. Less dry phases were likely caused by transiently increased influence of the westerlies and/or decreased influence of the Asian winter monsoon on glacial–interglacial time scales. An exception from this relationship is the interval between ~1.9 and 1.3 Ma, when the SG-1 χ record exhibits a 54 ka cyclicity, which may indicate summer monsoon influence on the Qaidam Basin during that time. After ~1.3 Ma, the summer monsoon influence may have ceased due to global cooling, with the consequence that the Asian winter monsoon and the westerlies exerted a stronger control on the hydrology of the Qaidam Basin.

Introduction

The Tibetan Plateau (TP) is the largest continental plateau on Earth, and its topography has a profound impact on the climate system of the Northern Hemisphere (Harrison et al., 1998; An et al., 2001). The amount of ice stored on the TP is the third largest on Earth after the Antarctic and Arctic cryospheres (Qiu, 2008). The region directly adjacent to the TP to the north, including the Tarim Basin, is today largely arid, and it has undergone increasing aridification during the Late Cenozoic (Guo et al., 2002; Tang et al., 2011). In this context, a better understanding of the hydrological cycle on the TP and adjacent regions, and notably its variability through time, is essential for improving predictions of future climate and ecosystem evolution.

The present-day climate on the TP is affected by the relative influences of the Indian and East Asian monsoon, the westerlies, and the Asian winter monsoon (Fig. 1; Bothe et al., 2012; Maussion et al., 2014; Mölg et al., 2014). The monsoon system is controlled by a pressure gradient in the troposphere and the role of the TP as an orographic barrier (Boos and Kuang, 2010; Molnar et al., 2010). Because the plateau acts as a topographic divide, the westerlies split into a northern and a southern branch in winter (Wang, 2006). Considerable knowledge of monsoon dynamics comes from the marine realm, particularly from well-dated marine drill cores (e.g., Clemens et al., 1991; Zhang et al., 2009; Ao et al., 2011). However, an increasing number of studies have focused on monsoon dynamics in Central Asia during the Cenozoic using terrestrial archives. Among these archives, glaciers (Yao et al., 2012), lake sediments (Wang et al., 1999; An et al., 2011; Hu et al., 2015), loess deposits (Bloemendal and Liu, 2005; Sun et al., 2010), and alluvial records (Licht et al., 2014) have played a prime role in deciphering the spatiotemporal variability of monsoonal influence on the TP and its borderlands. Prominent examples come from the Chinese Loess Plateau (Fig. 1; Sun et al., 2010; Nie et al., 2013) or the Heqing Basin on the southeastern TP (Fig. 1; An et al., 2011; Hu et al., 2015). However, continuous records of past environmental change on the TP and from its surroundings are still scarce, especially on longer time scales (i.e., millions of years); this holds particularly true for the semi-arid to arid northern part of the TP.

The Cenozoic drying is a major factor in the climate evolution of Central Asia (Ramstein et al., 1997; Guo et al., 2002; Tang et al., 2011).

* Corresponding author.
E-mail address: erwin.appel@uni-tuebingen.de (E. Appel).

http://dx.doi.org/10.1016/j.yqres.2015.09.009
0033-5894/

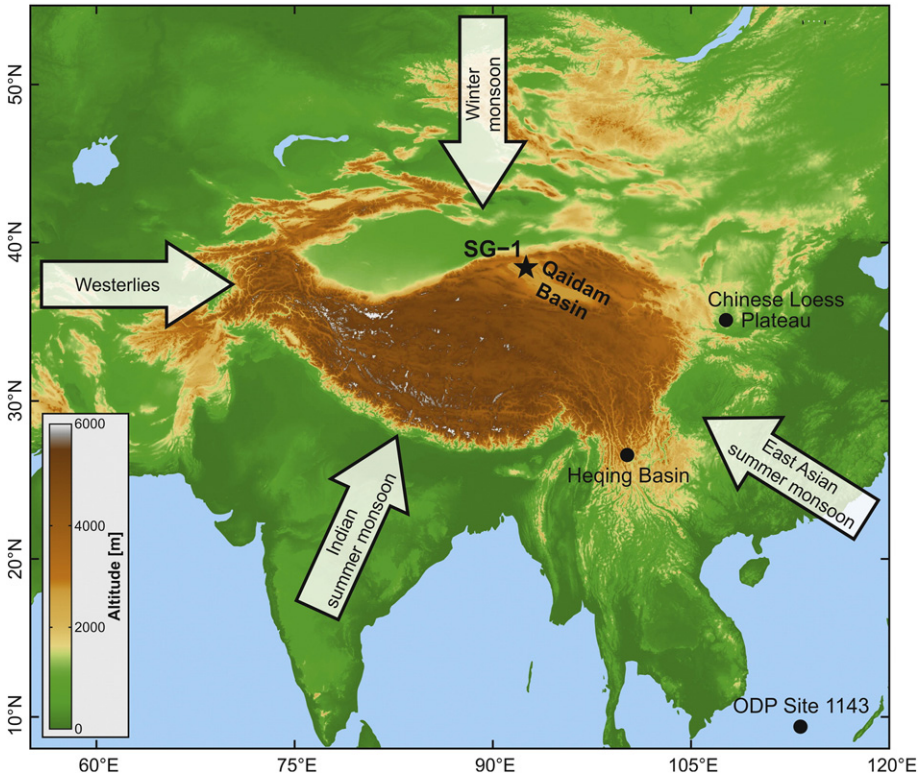

Figure 1. Tibetan Plateau with indicated global circulation pattern and the location of the drilling site SG-1. Locations of the proxy data sets mentioned in Fig. 4 are indicated: Indian summer monsoon (ISM) index from the Heqing Basin (An et al., 2011), hematite to goethite ratio (Hm/Gt) of ODP Site 1143 (Zhang et al., 2007, 2009; Ao et al., 2011), and the quartz mean grain size (QGS) from the southern Loess Plateau (Sun et al., 2010) (see also Fig. 4).

Possible main drivers of this aridification are global cooling, with a major step being connected to the Eocene–Oligocene transition (Wang et al., 1999; Guo et al., 2002; Dupont-Nivet et al., 2007) and progressive cooling starting after the Mid-Miocene Climatic Optimum (Zachos et al., 2001), the uplift and continuous elevation increase of the TP (Rowley and Currie, 2006; Dupont-Nivet et al., 2008; Liu and Dong, 2013), and the retreat of the Paratethys between Late Eocene and Late Miocene times (Ramstein et al., 1997; Guo et al., 2002; Dupont-Nivet et al., 2007). A similar mechanism was proposed recently by Buggle et al. (2013) for the observed aridification in SE Europe since the early Middle Pleistocene, i.e., in the region situated at the western end of the Eurasian steppe belt.

Among the large number of basins on the TP that have ultimately resulted from the India–Asia collision, the Qaidam Basin on the northeastern fringe of the plateau (Fig. 1) is one of the most prominent examples (Fang et al., 2007; Kapp et al., 2011; Zhang et al., 2013). Due to its geographical position and geological setting, it is ideally suited for investigating the long-term paleoclimate evolution of Central Asia. Firstly, the basin has been a closed system since at least Oligocene times, and alluvial and fluvio-lacustrine sedimentation was presumably almost continuous across much of the basin since the Eocene (Wang et al., 2012; Heermance et al., 2013). Secondly, the basin is located in a strategic position regarding the interplay between the westerlies, the Asian winter monsoon, and the Indian and East Asian monsoon; hence, paleoclimate archives from the basin can be considered to be particularly sensitive in recording climate change and its imprint on terrestrial ecosystems.

The present study focuses on the ~940-m-long drill core SG-1 (38°24′35″N, 92°30′33″E) that was drilled in 2008 in the Chahansilatu sub-basin of the western Qaidam Basin (Fig. 1) within a Sino–German cooperation project (Wang et al., 2012; Zhang et al., 2012b). A precise age model for the lacustrine sediments from core SG-1, hereafter termed 'SARA' age model, has been developed by Herb et al. (2015) based on orbital tuning of the mass-specific magnetic susceptibility (χ) record, and anchors from magnetostratigraphic (Zhang et al., 2012b) and optically stimulated luminescence data (Han et al., 2014b). The time interval spanned by core SG-1 includes the Middle Pleistocene Transition (MPT) (~1.25–0.7 Ma; Clark et al., 2006), which denotes a shift from 41-ka obliquity- to 100-ka eccentricity-dominated climate cycles (Head and Gibbard, 2005; Clark et al., 2006). The spectral shift of the MPT represents the main characteristic of the SG-1 χ time-series results (Herb et al., 2013, 2015).

Within the wide range of terrestrial paleoclimate proxies, pollens have proven to be one of the most useful groups. Their parent plants are highly responsive to climatic change, and they are abundant in a wide range of continental sedimentary settings, thus allowing a high spatio-temporal resolution of climate reconstructions (e.g., Birks and Birks, 1980; Pross et al., 2000). However, pollen analysis is extremely time-consuming. In contrast, χ can be measured very quickly, therefore enabling a high temporal resolution throughout a long sequence with a limited effort. Based on this rationale, Herb et al. (2013) have investigated the potential link between χ values and the humidity-sensitive *Artemisia*/Chenopodiaceae (A/C) pollen ratio across the depth interval from 403 to 278 m of the SG-1 core (Fig. 2a), which according to the SARA age model spans from 1.23 to 0.76 Ma. The A/C ratio is considered as a reliable proxy for humidity fluctuations in arid regions on the TP, including the Qaidam Basin, as *Artemisia* cannot tolerate as dry climates as Chenopodiaceae (Herzschuh, 2007; Zhao et al., 2012). The high informative value of the A/C ratio as a moisture indicator has previously been demonstrated for the Late Plio-Pleistocene of the western Qaidam Basin (Cai et al., 2012). For the analyzed portions of the SG-1 core (the 125-m-long interval between 403 and 278 m core depth), Herb et al. (2013) identified a pronounced inverse correlation between χ values and the A/C ratio.

In the present paper, we assess the pattern of moisture fluctuations over the entire SG-1 core, thereby extending the comparison of χ values and the A/C ratio as pioneered by Herb et al. (2013) for the MPT interval of the core to the entire Late Plio-Pleistocene. The resulting

https://doi.org/10.1016/j.yqres.2015.09.009 Published online by Cambridge University Press

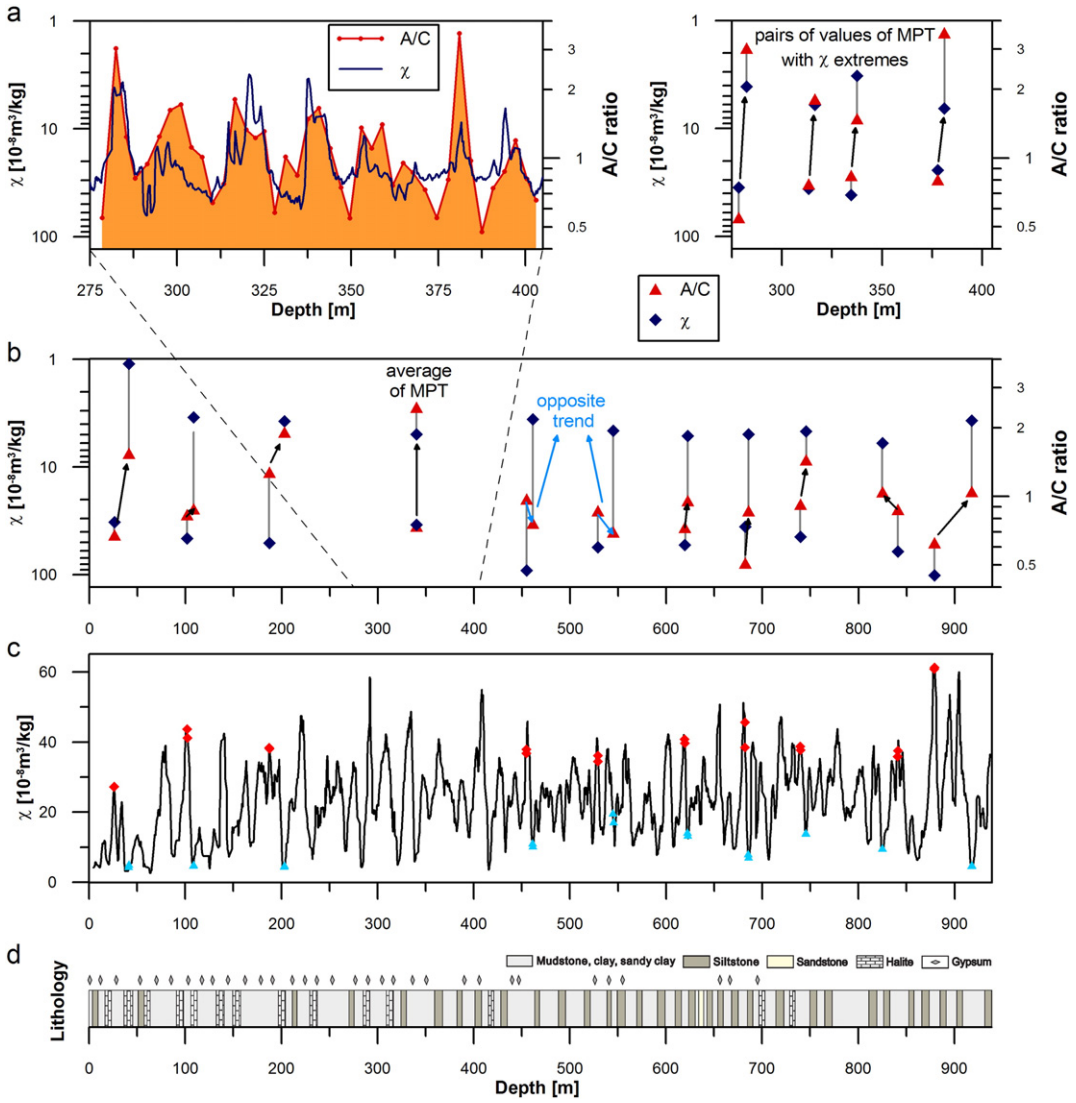

Figure 2. Relationship between magnetic susceptibility (χ; data from Zhang et al., 2012c) and the *Artemisia*/Chenopodiaceae (A/C) ratio, (a) around the MPT (adapted from Herb et al., 2013) with the smoothed (5-point simple moving average) χ depth series, and (b) for the additional pollen samples along the entire core. For the MPT average in (b), four pairs of values (small plot in (a)) at depth levels with extreme values of χ were averaged. Black arrows demonstrate a negative correlation of χ and A/C ratio, light blue arrows a positive correlation. In (c) the χ depth series is shown (11-point simple moving average; data from Zhang et al., 2012c) with the stratigraphic positions of the samples in the χ_l (blue) and χ_h group (red). (d) Core lithology (from Zhang et al., 2012b).

new high-resolution paleo-moisture dataset spans the entire time interval between 2.69 and 0.08 Ma. This dataset now allows us to identify the chronology of drier and less dry phases in the Qaidam Basin, to analyze the potential influence of the global climate system on paleo-precipitation in the Qaidam Basin, and to better understand the mechanisms leading to the exsiccation of the formerly extensive Qaidam paleolake during that time.

Study area

Geological setting

The Qaidam Basin is situated at the northeastern fringe of the TP, between 36–39°N and 90–98°E (Fig. 1). With an area of ca. 120,000 km^2 it is the largest intermontane basin on the TP, confined by the Qilian Shan (northeast), Kunlun Shan (south), and Altun Shan (northwest). These mountain ranges reach altitudes of >5000 m asl; the basin interior is on average at 2800 m asl. In addition to these topographic boundaries, the Qaidam Basin is tectonically bounded by the Qilian Shan–Nan Shan thrust belt (northeast), the eastern Kunlun thrust belt (south), and the Altyn Tagh fault (northwest) (Yin et al., 2008). Cenozoic lacustrine sediments originating from the surrounding mountains reach a thickness of >15,000 m in the basin center (Huang et al., 1996; Fang et al., 2007; Yin et al., 2007); near our study site in the western basin the lacustrine sediments are up to 6000 m thick (Zhang et al., 2012b, 2012c).

Climatic boundary conditions

The climate in the Qaidam Basin today is marked by hyper-aridity. The present-day mean annual precipitation over the basin is <50 mm/yr (Chen and Bowler, 1986) and mainly influenced by the westerlies (Bothe et al., 2012; Maussion et al., 2014). For the eastern part of the basin, an influence of the East Asian summer monsoon is debated (Li et al., 2006; Xu et al., 2011).

The Plio-Pleistocene evolution of moisture availability in the Qaidam Basin and its potential link to the Asian monsoon system has yet remained limited (e.g., Wang et al., 1999; Fang et al., 2008). The lacustrine sediment sequence of core SG-1 is well suited for studying past climate change in that region. The sedimentary sequence of core

https://doi.org/10.1016/j.yqres.2015.09.009 Published online by Cambridge University Press

SG-1 exhibits long-term changes in (a) lithology, such as an increasing presence of evaporites and a slight grain-size coarsening in the upper core intervals (Wang et al., 2012), and (b) sediment geochemistry, such as in Mn, U, and rare earth element concentrations (Yang et al., 2013a, 2014, 2015). Long-term changes in both the lithological and geochemical compositions of SG-1 suggest a stepwise aridification of the western Qaidam basin: In particular, lithofacies variations suggest intensification steps in the long-term aridification to have occurred at 2.5, 2.2, 1.6, 1.2, 0.9, 0.6, and 0.1 Ma (Wang et al., 2012); the different long-term stages of the Qaidam paleolake levels during the time covered by the SG-1 core as interpreted from lithofacies variation are (i) a semi-deep fresh to brackish lake between 2.8 and 2.5 Ma, (ii) a shallow brackish lake between 2.5 and 1.2 Ma, (iii) a shallow perennial saline lake between 1.2 and 0.6 Ma, and (iv) saline mudflats and playa saline lakes between 0.6 and 0.1 Ma (Wang et al., 2012). A stepwise aridification is further supported by variations in phosphorus concentration that indicate a long-term deterioration with increasing aridification at ~2.5, 1.8, 1.2, and 0.6 Ma (Yang et al., 2013b). Carbon isotope analyses covering the time span from 1.8 to 0.1 Ma support an increased drying at 1.2 and 0.6 Ma (Han et al., 2014a). Potential explanations for the enhanced exsiccation process since the Late Pliocene consider a link to an elevation increase of the TP and global cooling (Wu et al., 2011; Han et al., 2014a).

Today, gravel deserts, playas, salt lakes, yardangs, and shifting sands dominate the landscape in the western Qaidam Basin. The vegetation cover in the western Qaidam Basin consists of typical desert communities dominated by Chenopodiaceae, whereas the eastern parts of the basin exhibit a steppe vegetation with a strong presence of Poaceae (Zhao et al., 2007; Zhao and Herzschuh, 2009). More specifically, the vegetation in the surroundings of the SG-1 drill site consists predominantly of Chenopodiaceae; *Artemisia*, Poaceae, *Ephedra*, *Nitraria*, and *Tamarix* are also present; at higher altitudes of the surrounding mountains *Pinus*, *Picea*, and *Betula* occur (Zhao et al., 2007; Zhao and Herzschuh, 2009; Zhang et al., 2012a). Pollen analyses of Plio-Pleistocene (3.1–0.01 Ma) lacustrine sediments from the western Qaidam Basin (~65 km to the west of the SG-1 locality) revealed that *Artemisia* and Chenopodiaceae played a major role in vegetation during that time; compared with shrubs and herbs, tree taxa were of minor importance (Cai et al., 2012).

Material and methods

Material

The sedimentary succession of core SG-1 comprises predominantly mudstone and siltstone, salt layers (mainly at depths above ~420 m), and scattered gypsum crystals (Fig. 2d; compare also Wang et al., 2012, and Zhang et al., 2012b).

We selected ten pairs of samples from highs (χ_h group) and lows (χ_l group) in the χ variation (for positions in the sequence see Fig. 2c). In order to check for consistency of the magnetic and palynological results we investigated duplicate samples close to each other (on average within 0.3 m in depth). Thus, 40 (2×20) samples were investigated in total.

For a direct comparison of magnetic parameters with palynological data, pollen assemblages from these 40 samples were determined. They extend the already existing pollen dataset from the 403–278 m depth interval as presented by Herb et al. (2013) across the entire core SG-1. For pollen analysis we took samples that were previously used for χ measurements.

Methods

Magnetic properties

For the depth levels that were used for pollen analysis, we analyzed the following previously measured magnetic properties for their representativeness of the whole-core magnetic signature: mass-specific and frequency dependence of magnetic susceptibility (Zhang et al., 2012c), paramagnetic susceptibility (Herb et al., 2013), hysteresis properties (Herb et al., 2013), mass-specific susceptibility of anhysteretic remanent magnetization (Zhang et al., 2012c), and S-ratio (Zhang et al., 2012c). Additionally, we measured first-order reversal curves (FORCs), thermal demagnetization of saturation isothermal remanent magnetization (SIRM), and thermomagnetic (κ-T)-curves for each second sample. Hysteresis measurements were performed with a Micromag2900 AGM (Princeton Measurements Corporation); thermal demagnetization curves of the SIRM (acquired at 2.5 T; imparted with a pulse magnetizer MMPM9, Magnetic Measurements) was done in 16 steps up to 700°C using a shielded furnace MMTD (Magnetic Measurements) and using a Minispin magnetometer (Molspin) for intensity measurement; κ-T-curves were obtained with a Kappabridge MFK1-FA (AGICO) with an attached CS-3 furnace (max. 700°C). The determined FORCs include 100 partial hysteresis curves; the MATLAB code UNIFORC (Winklhofer and Zimanyi, 2006; Winklhofer et al., 2008; Egli et al., 2010) was used for processing (using a smoothing factor of 8 for the χ_l group and of 5 for the χ_h group); for samples with low χ FORC diagrams of three sub-samples were stacked. For detrending the χ time series we applied locally weighted scatterplot smoothing (LOWESS; Cleveland, 1979; Helsel et al., 2006).

Palynology

The pollen samples were prepared with the same techniques as used by Herb et al. (2013) including freeze drying, weighing, HCl (30%) and HF (40%) treatment, and sieving (using a 10 μm nylon mesh). At least 300 pollen grains were counted per sample using 400× magnification, except for four samples that yielded ≤50 pollen grains (at 25.61, 41.29, 187.56, and 681.92 m depth) and were excluded from further consideration (remaining samples: on average 317 grains counted). A precondition for using the A/C ratio as a humidity indicator is the amount of *Artemisia* and Chenopodiaceae adding up to at least >40–50% of the total pollen grains (Zhao et al., 2012). Because of this criterion, one sample had to be excluded from the interpretation (at 825.16 m depth). Another sample (at 102.30 m depth) was not considered because of an anomalous magnetic behavior (thermomagnetic curves of magnetic susceptibility, hysteresis properties, and mass-specific susceptibility of anhysteretic remanent magnetization). Nevertheless, at each sampled depth level at least one pollen sample was provided. For the 14 levels with duplicate results, the values from both samples were averaged. In addition to the newly available 34 samples, we also included the palynological results of the 41 samples discussed by Herb et al. (2013) in the short interval along the MPT in our analysis.

Results

Comparison of χ values and A/C ratio

The χ record features high-amplitude variation in the range of Milankovitch cycles (Herb et al., 2013, 2015) with the additional influence of long-term trends (Fig. 2c). Mean χ values of the χ_l group and χ_h group amount to 4.1×10^{-8} m^3/kg and 63.0×10^{-8} m^3/kg, respectively (Zhang et al., 2012c). In the accepted 34 samples *Artemisia* and Chenopodiaceae make up for an average of 57% (minimum: 47%, maximum: 69%) of total pollen grains. From a palynological perspective, this suggests the presence of typical desert to steppe vegetation throughout the Late Plio-Pleistocene. The mean A/C ratio is 1.10 (0.48–2.06; $\sigma = 0.42$) for the χ_l group and 0.83 (0.51–1.28; $\sigma = 0.19$) for the χ_h group (Fig. 2b). A visual comparison of χ and A/C ratios exhibits an anti-correlation between both variables, i.e., confirming the observation along the MPT (Herb et al., 2013). However, linear correlation does not yield a significant correlation coefficient. For linear correlation

https://doi.org/10.1016/j.yqres.2015.09.009 Published online by Cambridge University Press

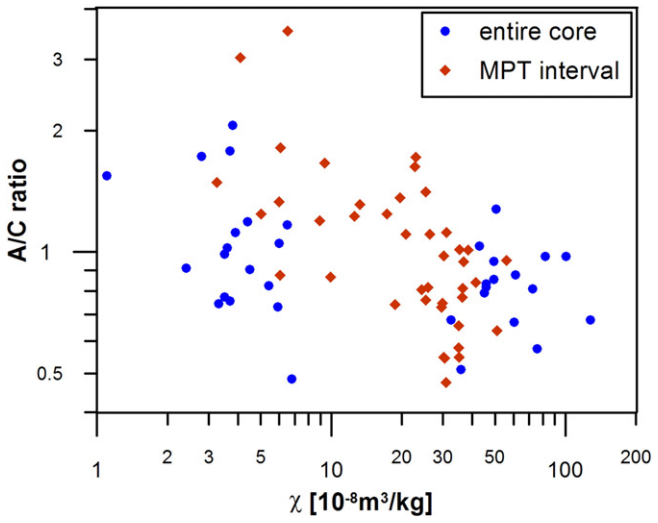

Figure 3. *Artemisia*/Chenopodiaceae (A/C) ratio versus magnetic susceptibility (χ; data from Zhang et al., 2012c) for the samples around the MPT (from Herb et al., 2013) and additional 34 values along the entire core (stratigraphic positions in Fig. 2c).

analysis three groups are considered: the 34 newly considered samples, the 41 samples around the MPT (Herb et al., 2013), and both groups together. A/C ratios and χ values (Fig. 3) show only a weak anti-correlation for the 34 new samples (Pearson's correlation coefficient $r = -0.34$) and for all samples ($r = -0.36$), and a moderate anti-correlation for the MPT samples ($r = -0.57$). This suggests a more complex relationship between the palynological and the magnetic signals. A close inspection reveals eight pairs of values from adjacent χ_l and χ_h samples showing an inverse relationship of χ and A/C ratios as revealed by Herb et al. (2013) for the MPT interval, while one interval with two pairs of values (at ~460 m and ~540 m) shows a positive relationship (Fig. 2b).

Magnetic characterization

The magnetic behavior of the samples in the χ_l and χ_h group was analyzed to show their representativeness and consistency. In addition to the previously discussed magnetic results (Zhang et al., 2012c; Herb et al., 2013), thermal demagnetization behaviors and thermomagnetic curves of magnetic susceptibility were investigated. We found that the properties of the samples used in this paper are in good agreement with previous results of samples with low and high χ values (Zhang et al., 2012c) and therefore do not present these results here in detail.

Previous observations of the linkage between χ and hysteresis loop properties revealed wider scattered magnetic grain sizes for lower χ samples than for higher ones (Zhang et al., 2012c; Herb et al., 2013). Thus, a wider range of magnetic grain sizes indicates less dry times (and vice versa) in consideration of the new χ–A/C ratio comparison. We investigated FORC diagrams for the verification of this linkage in addition to the previous hysteresis results because these enable an advanced characterization of magnetic phases in the sediments (Roberts et al., 2000; Rowan and Roberts, 2006). The new FORC results (see Supplementary online material) support the previous information on magnetic mineralogy and grain sizes gathered for core SG-1 (Zhang et al., 2012c; Herb et al., 2013).

Discussion

Magnetic susceptibility as a paleo-humidity proxy

As already mentioned in the Introduction, higher A/C ratios are related to less dry intervals and vice versa under such semi-arid to arid climate conditions. Values of χ and A/C ratios show an inverse relationship for the predominant part of core SG-1, covered by the newly analyzed samples (Fig. 2b). Hence, we conclude that low χ values indicate less dry conditions, whereas higher χ values indicate drier conditions throughout most of the time span of the SG-1 core.

The FORC results (see Supplementary online material) show a clear tendency of relatively larger magnetic grain sizes in the χ_l group (mainly multi-domain to pseudo-single-domain behavior) compared with the χ_h (mainly single-domain behavior). This is in agreement with low-temperature oxidation (LTO) as a major factor of weathering causing the alteration of magnetite to maghemite and finally a transformation to hematite (Sidhu, 1988; van Velzen and Dekkers, 1999; Buggle et al., 2014; Ge et al., 2014) as it was concluded by Zhang et al. (2012c) and Herb et al. (2013). LTO leads to lower χ values by partial transformation of magnetite/maghemite into hematite. It also explains the observed widening of the magnetic grain-size range in the χ_l sediments because of the predominant alteration of smaller grains because of their higher surface-to-volume ratios (Haneda and Morrish, 1977; van Velzen and Dekkers, 1999). When the initially predominant smaller grains are transformed to hematite, a pre-existing larger grain-size fraction of magnetite/maghemite naturally appears in the magnetic characteristics of the analyzed samples. Our new results indicate that the inverse relationship between χ and A/C values extends through the major part of core SG-1, but the correlation is weaker for the entire core than for the much shorter MPT interval. Besides LTO in the catchment area, changes in the source area also contributed to variability in the magnetic signal (Zhang et al., 2012c; Herb et al., 2013). The LTO scenario implies less dry conditions for phases with lower χ values and vice versa (Zhang et al., 2012c; Herb et al., 2013), but source area changes can be responsible for long-term biasing of the initial concentration and grain size of magnetite on which LTO works.

Implications of the χ–A/C relationship

Methodological implications

In light of the A/C ratio representing a reliable humidity proxy in the study area (Cai et al., 2012; Zhao et al., 2012) and its observed link to χ (Fig. 2), the variation of χ can be used as a climate proxy for the arid environment of the investigated region as proposed by Herb et al. (2013) for the much shorter MPT interval. Eventually, owing to the new χ–A/C ratio comparison along the entire SG-1 core, χ can be considered as a first-order moisture proxy during persistently dry conditions. However, such an interpretation is only possible for the shorter-term cycles of χ and not by a linear correlation on a long-term scale. The relation between χ and the A/C ratio is complex, as indicated by the relatively low linear correlation coefficient of the overall sample set, and requires special attention for its analysis. Across the entire core, the absolute value of the Pearson's correlation coefficient is clearly lower than for the much shorter MPT interval alone. Thus, we speculate that the lower correlation reflects a non-linear magnetic response to climate associated with local or regional boundary conditions, such as changes in the catchment area. Variation in climate and lake-system conditions controls weathering and leads to different degrees of LTO. This could explain the inverse relationship of χ and A/C values for the shorter-term χ variation in the range of Milankovitch cycles. On a longer-term scale we have to consider changes in the sediment source area, like tectonic activity and the ongoing aridification process, which can shift the level of χ values and downgrading a direct correlation of χ and the A/C ratio for a whole-core comparison. Such changes of the catchment are potentially evoked by a shrinkage of the lake coming along with a change of the magnetic signature of the sediment source area. Longer-term influences by catchment changes become especially clear in the trend of the χ record (Fig. 4a) indicating an increase in humidity since ~0.8 Ma, but the opposite is evident from lithological observations (Wang et al., 2012). For that reason only nearby located pairs of values are observed in Figure 2b rather than values along the entire core as in Figure 3. The

https://doi.org/10.1016/j.yqres.2015.09.009 Published online by Cambridge University Press

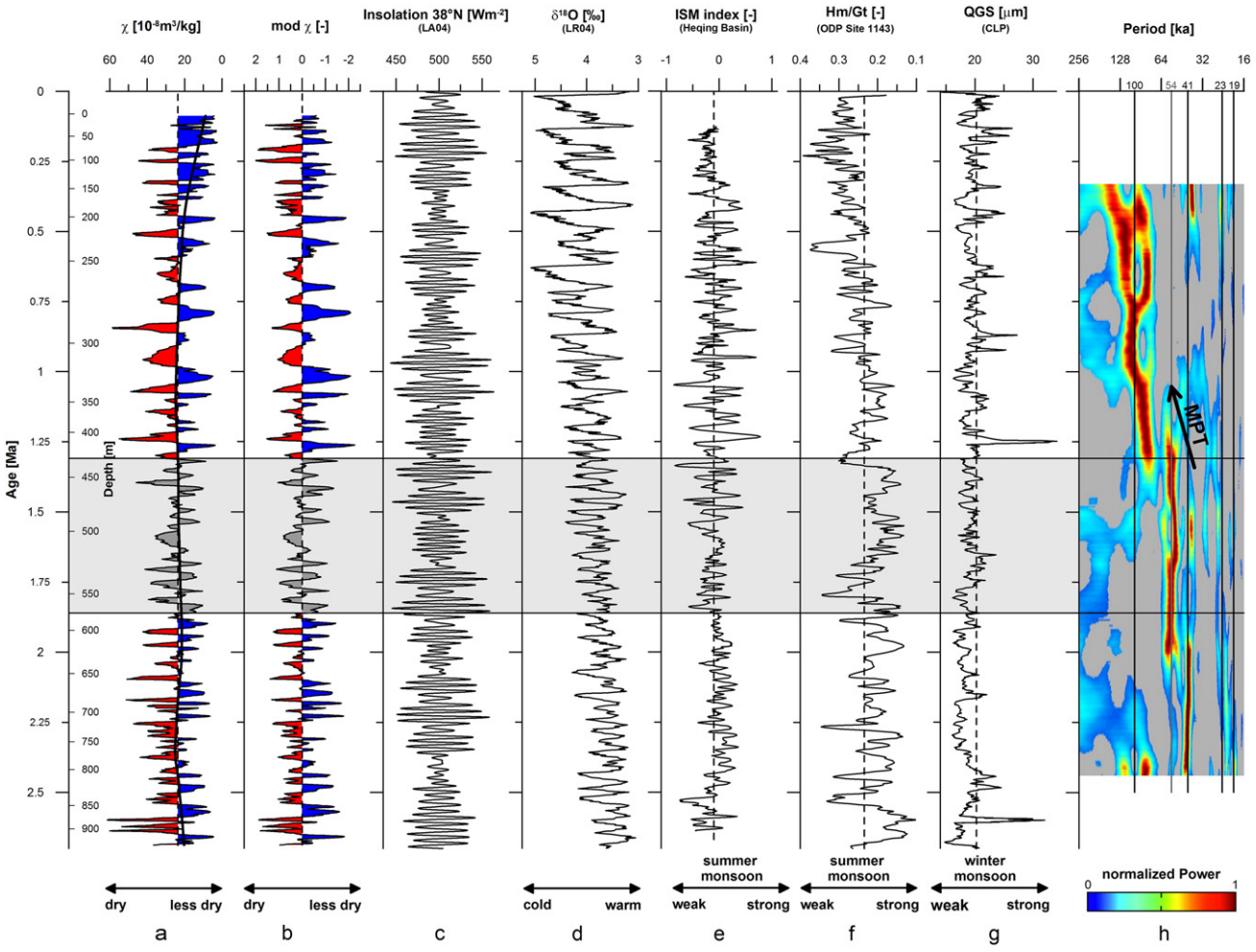

Figure 4. Magnetic susceptibility (χ; data from Zhang et al., 2012c) time series (11-pt simple moving average smoothed) using the SARA age model of Herb et al. (2015) for depth-time transformation; (a) original χ values (trend using locally weighted scatterplot smoothing (LOWESS) indicated by the black line) and (b) after detrending (by LOWESS) and normalizing (logarithmized and standard scores); dry and less dry phases according to the χ–A/C-ratio comparison (see Fig. 2) are indicated (the gray shaded part marks the interval with opposite χ–A/C-ratio relationship; the extent of this interval is determined by mid-point ages to the neighboring samples); (c) insolation curve for 38°N from the numerical solution LA04 by Laskar et al. (2004) for the summer solstice; (d) stacked benthic $\delta_{18}O$ record LR04 (Lisiecki and Raymo, 2005); (e) Indian summer monsoon (ISM) index from the Heqing Basin (SE Tibetan Plateau) (An et al., 2011); (f) ratio between the contents of hematite and goethite (Hm/Gt) of ODP Site 1143 (South China Sea) (Zhang et al., 2007, 2009; Ao et al., 2011); (g) quartz mean grain size (QGS) from the southern Loess Plateau (Sun et al., 2010). ISM index, Hm/Gt ratio, and QGS are 5-point moving average smoothed. (h) Spectral analysis of χ in sliding window with lengths of 500 ka in 5-ka resolution, power below red noise in gray (adapted from Herb et al., 2015). The interval with the 'opposite' χ–A/C behavior is marked by the gray-shaded background.

ambiguous interpretation of absolute χ values becomes clear in the MPT interval (Fig. 2a) for which we have higher-resolution pollen data. Also in this interval extreme values of the A/C ratio are represented by highly differing absolute χ values, but we have a convincing inverse relationship of the principle χ and A/C ratio cycles, without a recognizable phase shift (Herb et al., 2013).

Kapp et al. (2011) suggested strong wind erosion in the Qaidam Basin since the Late Pliocene. Such erosion processes likely led to a change of the sedimentary characteristics, which may explain the trend in the χ time series since ~0.6 Ma that is opposing the χ–A/C relationship. During the time interval since 0.6 Ma as covered by core SG-1, the Qaidam paleolake was exposed to pronounced drying near the SG-1 drilling site, which is manifested in the formation of playas (Wang et al., 2012). As a consequence of the playa formation, the source area for the sediments in core SG-1 likely altered through the erosion of the exposed material and related transport processes. The sediments delivered to the SG-1 drilling site by erosion processes likely had a different magnetic signature, which might have caused the opposing χ trend since ~0.6 Ma. In addition to the possible alteration of the sedimentary signature through the erosion of playas, the formation of anticlines in the basin could have led to an overprint of the sediment properties by causing a secondary sedimentary source area. The development of anticline structures is a common process in the western Qaidam basin due to continuous tectonic SW–NE compression (Xia et al., 2001; Yin et al., 2008; Lu et al., 2015). The growth of these anticlines has an impact on the sediment flux in the lake by forming sub-basins and sub-bottom slopes, and they become exposed to wind erosion when they rise over the lake level. The influence of a changing sedimentary source area could have strongly superposed the periodic humidity signal. A possible consequence for the χ–A/C-ratio behavior is discussed below.

Connection between χ and global climate records

To determine the driving factors of moisture changes in the western Qaidam Basin, we have compared the χ record with both global climate records and monsoon records. The χ time series (Fig. 4a) shows a clear cyclic behavior, with shorter cycles in the obliquity band dominating from the bottom of the core well into the MPT interval, and longer cycles in the eccentricity band dominating afterwards (Herb et al., 2015). As the MPT is a consistent feature of Quaternary climate records both from marine and terrestrial archives world-wide (Head and Gibbard,

https://doi.org/10.1016/j.yqres.2015.09.009 Published online by Cambridge University Press

2005), the documentation of the MPT in the χ record demonstrates a connection of the climate in the western Qaidam Basin to global climate conditions.

One possible explanation for the MPT is that Northern Hemisphere ice volume caused a change from linear to non-linear climate forcing when it exceeded a critical level (Imbrie et al., 1993; Abe-Ouchi et al., 2013). Following this hypothesis, we might assume that χ is at least indirectly influenced by ice-sheet dynamics. To potentially quantify such an influence we carried out a cross-spectral analysis of the SG-1 χ record with the numerically determined insolation (38°N; summer solstice) LA04 (Laskar et al., 2004; Fig. 4c) and the benthic $\delta^{18}O$ stack LR04 (Lisiecki and Raymo, 2005; Fig. 4d). Significant (95% level) coherence is detected between χ and LA04 for 41-ka obliquity (Fig. 5a). The 54-ka obliquity also shows a coherence peak; nevertheless, this is below the 95% significance level. A linear relationship between χ and LR04 in the frequency domain is significant (95% level) for the 41-ka obliquity, while coherence for the 54-ka cyclicity is slightly shifted to higher frequencies (Fig. 5b). Precession and eccentricity show less coherence in both cases, probably due to the separation of spectral power of χ into split peaks (Fig. 5). The cross-spectral analysis suggests a significant influence of insolation (LA04) on χ as well as a link to glacial–interglacial cycles represented by the LR04 stack. However, the observed dry and less dry phases (Fig. 4a, b) do not match chronologically with the expected glacial–interglacial periods shown by the LR04 stack (Fig. 4d). The time interval of the SG-1 χ record shown in Figure 4 is based on the SARA age model as it was developed by Herb et al. (2015) through orbital tuning of SARs. This tuning can cause shifts of the resulting absolute ages on the order of a few 10 ka, which hinders the direct chronological comparison with the LR04 stack.

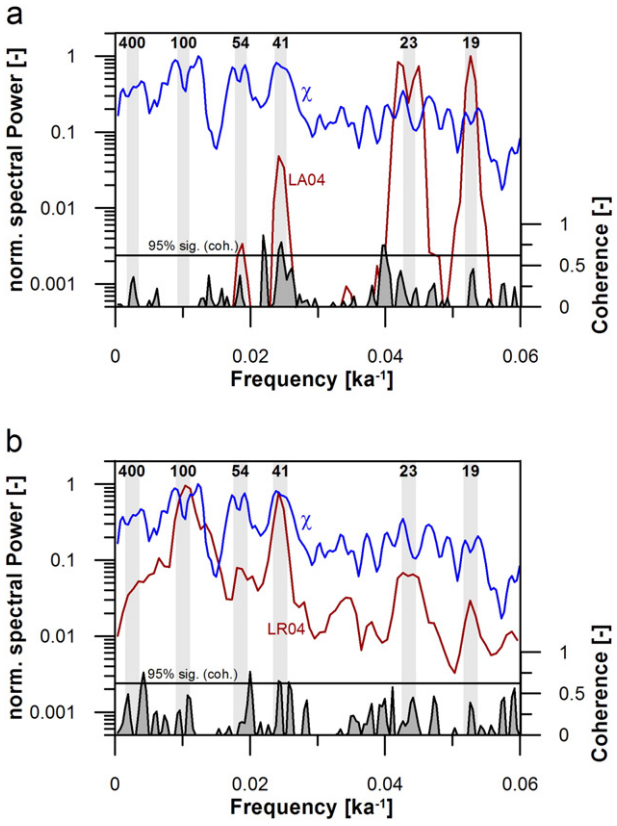

Figure 5. Cross-spectral analysis of magnetic susceptibility (χ; blue) with (a) LA04 (red; Laskar et al., 2004) and (b) LR04 (red; Lisiecki and Raymo, 2005), both shown for the same time span as covered by the SG-1 χ record (see Fig. 4); width of gray vertical bars reflect 6-dB bandwidth. SPECTRUM software (Schulz and Stattegger, 1997) was used for calculation after normalizing (log transformation and standard scores).

'Anomaly' of the χ versus A/C-ratio relationship

In the interval between ~1.9 and ~1.3 Ma, two pairs of χ and A/C values show a positive correlation in contrast to all other samples, for which an inverse correlation is observed (Fig. 2). The occurrence of this 'anomaly' within one interval indicates that it represents a systematic difference rather than an effect of scattering. The reason for this systematic difference is likely a change of the boundary conditions (like shifts of the catchment area) as discussed above. Based on the predominantly A/C-ratio-based climate reconstructions for the western Qaidam Basin as presented by Cai et al. (2012), the anomalous behavior of the χ versus A/C values falls within an interval of less dry conditions that lasted from 1.8 to 1.2 Ma. Therefore, we assume that the anomalous χ–A/C-ratio behavior is evoked by less dry conditions in that time, which resulted in a longer-term change of the magnetic signature likely due to different boundary conditions.

Less dry times in the anomalous interval could be caused by long-term changes in the precipitation reaching the western Qaidam Basin, potentially due to tectonic forcing (i.e., uplift and consequently increasing elevation of mountain ranges surrounding the basin; Song et al., 2005; Yin et al., 2008), shifts of the intertropical convergence zone (Fleitmann et al., 2007), variations in monsoon intensity (Bolton et al., 2013), and/or a combination of these factors. In the following, we will investigate how changes in monsoonal intensity may have affected the moisture budget in the western Qaidam Basin. Based on lacustrine sediments from the Heqing Basin, An et al. (2011) quantified the strength of the Indian summer monsoon (ISM) reaching the southeastern TP for the period from 2.6 to 0.1 Ma. Their ISM index (Fig. 4e) shows an increase in amplitudes at around 1.6 Ma, which coincides with the middle part of the 'anomalous' interval of the SG-1 record as described above. Moreover, the 'anomalous' interval falls within a period of a relatively strong Asian summer monsoon as identified from marine sediments at ODP Site 1143 in the South China Sea (Fig. 4f; Zhang et al., 2007, 2009; Ao et al., 2011). Precipitation directly related with monsoon circulation seems unlikely in the western Qaidam Basin owing to its position on the northeastern edge of the TP. However, the larger-scale atmospheric circulation affecting the Qaidam Basin could be coupled to the summer monsoon system, at least in certain periods during which such an influence was supported by the atmospheric circulation pattern. Temporary coupling of the climate in the western Qaidam Basin with the summer monsoon system could have caused climate conditions that biased the sediment supply to the lake. This may have changed the magnetic signature generating the contrary χ–A/C-ratio behavior in the anomalous interval. According to Clemens and Prell (1991) a potential link between the 54-ka cycles and summer monsoon strength might exist, attributed to feedback effects of the climate system with the assumption that the 54-ka cyclicity results from a combination of the primary precession and obliquity cycles. Herb et al. (2015) have identified the 54-ka cycle as the dominant periodicity in the χ record of the SG-1 drill core (Fig. 4h) for the period ~2.0–1.3 Ma. This period coincides with the discussed anomalous interval and thus may support a coupling of the climate in the western Qaidam Basin to the summer monsoon system during that time.

Bringing dry air masses from the north and also influencing the summer monsoon (Chen et al., 2000) the winter monsoon is another important climate feature in Central Asia today. Winter monsoon intensity was reconstructed for the past 7 Ma on the southern Loess Plateau (Fig. 4g; Sun et al., 2010) based on the size distribution of quartz grains (Xiao et al., 1995). For the 'anomalous' interval, the grain-size data indicate a relatively weak winter monsoon with only small-amplitude variations (Sun et al., 2010). This observation further supports the scenario that less dry conditions may have been responsible for the inverse pattern of the χ and A/C values in the 'anomalous' interval.

https://doi.org/10.1016/j.yqres.2015.09.009 Published online by Cambridge University Press

The observed 'anomaly' might also be explained by anticline formation in the area influencing the sedimentary characteristics of core SG-1, as already addressed above. In this respect, the Jianshan anticline is of particular interest as it is only at ~20 km distance to the SG-1 drill site. The ultimate uplift above lake level occurred at ~1.6 Ma (Zhang et al., 2014; Lu et al., 2015), i.e., during the phase of the opposite χ–A/C-ratio (between ~1.9 and ~1.3 Ma); however, a temporary rise above lake level might have started already earlier. In such a scenario, the sedimentary system in the area of the SG-1 drill site likely took some time to re-equilibrate until humidity fluctuations returned to the primary influencing factors of the χ variation. Nevertheless, the accordance with other summer monsoon records (Sun et al., 2010; An et al., 2011; Ao et al., 2011) and the observation of the 54-ka orbital cycle throughout the period of the 'anomaly' suggest a link of the χ record to the moisture availability in the Qaidam Basin and the monsoon system rather than an overlay of the magnetic signal by sediments from the Jianshan anticline.

Environmental implications

Global cooling presumably caused a strengthening of the Siberian High (Guo et al., 2004), leading to an increased strength of the dry-cold winter monsoon, a decrease in the importance of the summer monsoon for the Qaidam Basin (Fang et al., 1999), and a reduction of the moisture transported to inner Asia by the westerlies (Yang et al., 2013b). In addition to these processes, uplift and continuous elevation increase of the TP may also have led to a stronger winter monsoon and the enhancement of the westerlies (Ruddiman and Kutzbach, 1989; Fang et al., 1999), thereby contributing to the increasing aridification since ~1.2 Ma (Fang et al., 1999; Han et al., 2014a). As a result of a reduced moisture flux into Central Asia, the regional climate in the Qaidam Basin became increasingly separated from the surroundings since ~1.2 Ma. The basin was closed during that time (Wang et al., 2012), thus direct outward flow did not take place. Due to the high mountain ranges surrounding the basin, the transport of water vapor out of the basin seems also being limited. Therefore, the water cycle in the basin itself is likely very important. We hypothesize that the aridification process observed in SG-1 was controlled by regional water recycling (see next section). In such a scenario, insolation changes influence the moisture budget in the Qaidam Basin on glacial–interglacial time scales as documented in the χ record of SG-1 via the occurrence of Milankovitch cycles.

Buggle et al. (2013) discussed an effect of progressive aridification due to an elevation increase of surrounding mountain belts in basins of SE Europe since the early Middle Pleistocene. Strong uplift processes of the NE Tibetan Plateau are assumed for the period around the MPT (Song et al., 2005; Liu et al., 2010; Zhang et al., 2012b). In the light of the interpretation of Buggle et al. (2013), the elevation increase of the surrounding mountain belts might also be responsible for the increasing aridification trend in the Qaidam Basin.

Outlook: aridification and regional water recycling

In the following, we propose a hypothesis that consistently explains the paleohydrological data represented by χ as well as a potential driving mechanism of the pronounced drying process in the western Qaidam Basin since the MPT. The formerly large paleolake in the Qaidam Basin and the region surrounding the basin may have formed a long-term, climate-driven closed water cycle, including evapotranspiration, precipitation and surface runoff, with a balance between moisture loss through the atmosphere and external moisture influx from the westerlies. In such a scenario, glacial and interglacial times will modulate the water budget by varying the volumes of lake water and glacier ice, with less precipitation during cooler periods. As long as the lake surface remained rather constant, such cycling could have been stable, causing drier or less dry conditions in the catchment area of the lake on a glacial–interglacial time scale.

As a consequence of stronger eccentricity control after the MPT in the study region (Fig. 4h; Herb et al., 2015), longer glacial periods with lengths between ~85 and 90 ka compared with the total 100 ka (Berger and Loutre, 2010) are expected for the younger half of the Quaternary. This period is the time span when drying in the Qaidam Basin intensified strongly (Wang et al., 2012). Therefore, a link between eccentricity control of humidity in the western Qaidam Basin since the MPT and the drying process of the Qaidam paleolake might exist. When water was detracted from the lake for longer times in the glacial periods since the MPT and the lake surface area was additionally reduced by the uplift of anticlines (Xia et al., 2001; Yin et al., 2008), a critical state could have been reached where the regional water recycling system collapsed leading to final drying of the paleolake. A similar process of hydrological water and moisture recycling has been suggested to explain present observations in the TP region (Chen et al., 2012; Mölg et al., 2014).

Conclusions

(1) New pollen results extend the previous comparison of χ and the A/C pollen ratio around the MPT to the entire core SG-1 (2.69–0.08 Ma). As for the MPT interval, higher χ values represent drier conditions and vice versa. Only the interval between 1.9 and 1.3 Ma shows the opposite relationship. Based on our pollen results, predominantly desert and steppe vegetation dominated the landscape in the study region during the ~2.61 Ma covered by core SG-1. The new palynological results as well as the analyzed FORCs verify the previous assumption that χ variation is based on both low-temperature oxidation occurring in the catchment and a changing source region of sediment supply controlling the long-term trends.

(2) Cross-spectral analysis suggests a high influence of insolation on the observed χ variation and a connection to glacial–interglacial cycles. From spectral analysis of the proposed paleo-humidity proxy χ we hypothesize that during the eccentricity-dominated glacial/interglacial cycles after the MPT, aridity increased by accumulation of water in glacier ice, leading to an almost complete exsiccation of the Qaidam paleolake after a tipping point was reached.

(3) Low intensity of the dry winter monsoon and evidence of monsoon-influenced moisture provides evidence for the summer monsoon as an important factor of climate control in the western Qaidam Basin during the time period with the opposite χ–A/C-ratio behavior (1.9–1.3 Ma). Based on the significance of the 54-ka cycle before 1.3 Ma as observed in our χ data, we speculate that fluctuations of drier and less dry climate in the Qaidam Basin were coupled to summer monsoon dynamics at least until the MPT.

Acknowledgments

Drilling of core SG-1 and this study was supported by the Priority Program 1372 ("Tibetan Plateau: Formation, Climate, Ecosystems") of the German Research Foundation (DFG; AP34/34; PR651/8), the German Federal Ministry of Education and Research (BMBF; 03G0705A), the National Natural Science Foundation of China (NSFC; 41321061, 41172032, 40702006), and the National Basic Research Program of China 973 (2011CB403000). We thank Dongliang Liu, Qibo Zhang, Shiyuan Li, Sihu Hu, Yibo Yang, and Yongbiao Yang for their support during fieldwork and Michael Winklhofer for the UNIFORC MATLAB code.

Appendix A. Supplementary data

Supplementary data to this article can be found online at http://dx.doi.org/10.1016/j.yqres.2015.09.009.

References

Abe-Ouchi, A., Saito, F., Kawamura, K., Raymo, M.E., Okuno, J., Takahashi, K., Blatter, H., 2013. Insolation-driven 100,000-year glacial cycles and hysteresis of ice-sheet volume. Nature 500, 190–193.

An, Z.S., Kutzbach, J.E., Prell, W.L., Porter, S.C., 2001. Evolution of Asian monsoons and phased uplift of the Himalaya–Tibetan plateau since Late Miocene times. Nature 411, 62–66.

An, Z.S., Clemens, S.C., Shen, J., Qiang, X.O., Jin, Z.D., Sun, Y.B., Prell, W.L., Luo, J.J., Wang, S.M., Xu, H., Cai, Y.J., Zhou, W.J., Liu, X.D., Liu, W.G., Shi, Z.G., Yan, L.B., Xiao, X.Y., Chang, H., Wu, F., Ai, L., Lu, F.Y., 2011. Glacial–interglacial Indian summer monsoon dynamics. Science 333, 719–723.

Ao, H., Dekkers, M.J., Qin, L., Xiao, G.Q., 2011. An updated astronomical timescale for the Plio-Pleistocene deposits from South China Sea and new insights into Asian monsoon evolution. Quaternary Science Reviews 30, 1560–1575.

Berger, A., Loutre, M.F., 2010. Modeling the 100-kyr glacial–interglacial cycles. Global and Planetary Change 72, 275–281.

Birks, H.J.B., Birks, H.H., 1980. Quaternary Palaeoecology. Edward Arnold, London.

Bloemendal, J., Liu, X.M., 2005. Rock magnetism and geochemistry of two Plio-Pleistocene Chinese loess-palaeosol sequences — implications for quantitative palaeoprecipitation reconstruction. Palaeogeography Palaeoclimatology Palaeoecology 226, 149–166.

Bolton, C.T., Chang, L., Clemens, S.C., Kodama, K., Ikehara, M., Medina-Elizalde, M., Paterson, G.A., Roberts, A.P., Rohling, E.J., Yamamoto, Y., Zhao, X.A., 2013. A 500,000 year record of Indian summer monsoon dynamics recorded by eastern equatorial Indian Ocean upper water-column structure. Quaternary Science Reviews 77, 167–180.

Boos, W.R., Kuang, Z.M., 2010. Dominant control of the South Asian monsoon by orographic insulation versus plateau heating. Nature 463, 218–222.

Bothe, O., Fraedrich, K., Zhu, X.H., 2012. Precipitation climate of Central Asia and the large-scale atmospheric circulation. Theoretical and Applied Climatology 108, 345–354.

Buggle, B., Hambach, U., Kehl, M., Marković, S.B., Zöller, L., Glaser, B., 2013. The progressive evolution of a continental climate in southeast-central European lowlands during the Middle Pleistocene recorded in loess paleosol sequences. Geology 41, 771–774.

Buggle, B., Hambach, U., Müller, K., Zöller, L., Marković, S.B., Glaser, B., 2014. Iron mineralogical proxies and Quaternary climate change in SE-European loess–paleosol sequences. Catena 117, 4–22.

Cai, M.T., Fang, X.M., Wu, F.L., Miao, Y.F., Appel, E., 2012. Pliocene–Pleistocene stepwise drying of Central Asia: evidence from paleomagnetism and sporopollen record of the deep borehole SG-3 in the western Qaidam Basin, NE Tibetan Plateau. Global and Planetary Change 94–95, 72–81.

Chen, K.Z., Bowler, J.M., 1986. Late Pleistocene evolution of salt lakes in the Qaidam Basin, Qinghai province, China. Palaeogeography Palaeoclimatology Palaeoecology 54, 87–104.

Chen, W., Graf, H.-F., Huang, R.H., 2000. The interannual variability of East Asian Winter Monsoon and its relation to the summer monsoon. Advances in Atmospheric Sciences 17, 48–60.

Chen, B., Xu, X.-D., Yang, S.A., Zhang, W., 2012. On the origin and destination of atmospheric moisture and air mass over the Tibetan Plateau. Theoretical and Applied Climatology 110, 423–435.

Clark, P.U., Archer, D., Pollard, D., Blum, J.D., Rial, J.A., Brovkin, V., Mix, A.C., Pisias, N.G., Roy, M., 2006. The middle Pleistocene transition: characteristics, mechanisms, and implications for long-term changes in atmospheric pCO_2. Quaternary Science Reviews 25, 3150–3184.

Clemens, S.C., Prell, W.L., 1991. Late Quaternary forcing of Indian Ocean summer-monsoon winds: a comparison of Fourier model and general circulation model results. Journal of Geophysical Research 96, 22683–22700.

Clemens, S., Prell, W., Murray, D., Shimmield, G., Weedon, G., 1991. Forcing mechanisms of the Indian Ocean monsoon. Nature 353, 720–725.

Cleveland, W.S., 1979. Robust locally weighted regression and smoothing scatterplots. Journal of the American Statistical Association 74, 829–836.

Dupont-Nivet, G., Krijgsman, W., Langereis, C.G., Abels, H.A., Dai, S., Fang, X.M., 2007. Tibetan plateau aridification linked to global cooling at the Eocene–Oligocene transition. Nature 445, 635–638.

Dupont-Nivet, G., Hoorn, C., Konert, M., 2008. Tibetan uplift prior to the Eocene–Oligocene climate transition: evidence from pollen analysis of the Xining Basin. Geology 36, 987–990.

Egli, R., Chen, A.P., Winklhofer, M., Kodama, K.P., Horng, C.S., 2010. Detection of noninteracting single domain particles using first-order reversal curve diagrams. Geochemistry, Geophysics, Geosystems 11. http://dx.doi.org/10.1029/2009GC002916 (Q01Z11).

Fang, X.M., Li, J.J., Van der Voo, R., 1999. Rock magnetic and grain size evidence for intensified Asian atmospheric circulation since 800,000 years B.P. related to Tibetan uplift. Earth and Planetary Science Letters 165, 129–144.

Fang, X.M., Zhang, W.L., Meng, Q.Q., Gao, J.P., Wang, X.M., King, J., Song, C.H., Dai, S., Miao, Y.F., 2007. High-resolution magnetostratigraphy of the Neogene Huaitoutala section in the eastern Qaidam Basin on the NE Tibetan Plateau, Qinghai Province, China and its implication on tectonic uplift of the NE Tibetan Plateau. Earth and Planetary Science Letters 258, 293–306.

Fang, X.M., Wu, F.L., Han, W.X., Wang, Y.D., Zhang, X.Z., Zhang, W.L., 2008. Plio-Pleistocene drying process of Asian inland — sporopollen and salinity records from Yahu section in the central Qaidam Basin. Quaternary Sciences 28, 874–882 (in Chinese).

Fleitmann, D., Burns, S.J., Mangini, A., Mudelsee, M., Kramers, J., Villa, I., Neff, U., Al-Subbary, A.A., Buettner, A., Hippler, D., Matter, A., 2007. Holocene ITCZ and Indian monsoon dynamics recorded in stalagmites from Oman and Yemen (Socotra). Quaternary Science Reviews 26, 170–188.

Ge, K.P., Williams, W., Liu, Q.S., Yu, Y.J., 2014. Effects of the core–shell structure on the magnetic properties of partially oxidized magnetite grains: experimental and micromagnetic investigations. Geochemistry, Geophysics, Geosystems 15, 2021–2038.

Guo, Z.T., Ruddiman, W.F., Hao, Q.Z., Wu, H.B., Qiao, Y.S., Zhu, R.X., Peng, S.Z., Wei, J.J., Yuan, B.Y., Liu, T.S., 2002. Onset of Asian desertification by 22 Myr ago inferred from loess deposits in China. Nature 416, 159–163.

Guo, Z.T., Peng, S.Z., Hao, Q.Z., Biscaye, P.E., An, Z.S., Liu, T.S., 2004. Late Miocene–Pliocene development of Asian aridification as recorded in the Red-Earth Formation in northern China. Global and Planetary Change 41, 135–145.

Han, W.X., Fang, X.M., Ye, C.C., Teng, X.H., Zhang, T., 2014a. Tibet forcing Quaternary stepwise enhancement of westerly jet and central Asian aridification: carbonate isotope records from deep drilling in the Qaidam salt playa, NE Tibet. Global and Planetary Change 116, 68–75.

Han, W.X., Ma, Z.B., Lai, Z.P., Appel, E., Fang, X.M., Yu, L.P., 2014b. Wind erosion on the NE Tibetan Plateau: constraints from OSL and U–Th dating of playa salt crust in the Qaidam Basin. Earth Surface Processes and Landforms 39, 779–789.

Haneda, K., Morrish, A.H., 1977. Vacancy ordering in γ-Fe_2O_3 small particles. Solid State Communications 22, 779–782.

Harrison, T.M., Yin, A., Ryerson, F.J., 1998. Orographic evolution of the Himalaya and Tibetan Plateau. In: Crowley, T.J., Burke, K. (Eds.), Tectonic Boundary Conditions for Climate Reconstructions. Oxford University Press, Oxford, pp. 39–72.

Head, M.J., Gibbard, P.L., 2005. Early–Middle Pleistocene transitions: an overview and recommendation for the defining boundary. In: Head, M.J., Gibbard, P.L. (Eds.), Early–Middle Pleistocene Transitions: The Land–Ocean Evidence. Geological Society, London, pp. 1–18.

Heermance, R.V., Pullen, A., Kapp, P., Garzione, C.N., Bogue, S., Ding, L., Song, P.P., 2013. Climatic and tectonic controls on sedimentation and erosion during the Pliocene–Quaternary in the Qaidam Basin (China). Geological Society of America Bulletin 125, 833–856.

Helsel, D.R., Mueller, D.K., Slack, J.R., 2006. Computer Program for the Kendall Family of Trend Tests. U.S. Geological Survey, Reston.

Herb, C., Zhang, W.L., Koutsodendris, A., Appel, E., Fang, X.M., Pross, J., 2013. Environmental implications of the magnetic record in Pleistocene lacustrine sediments of the Qaidam Basin, NE Tibetan Plateau. Quaternary International 313–314, 218–229.

Herb, C., Appel, E., Voigt, S., Koutsodendris, A., Pross, J., Zhang, W.L., Fang, X.M., 2015. Orbitally tuned age model for the Late Pliocene–Pleistocene lacustrine succession of drill core SG-1 from the western Qaidam Basin (NE Tibetan Plateau). Geophysical Journal International 200, 35–51.

Herzschuh, U., 2007. Reliability of pollen ratios for environmental reconstructions on the Tibetan Plateau. Journal of Biogeography 34, 1265–1273.

Hu, S.Y., Goddu, S.R., Herb, C., Appel, E., Gleixner, G., Wang, S.M., Yang, X.D., Zhu, X.H., 2015. Climate variability and its magnetic response recorded in a lacustrine sequence in Heqing basin at the SE Tibetan Plateau since 900 ka. Geophysical Journal International 201, 444–458.

Huang, Q.H., Huang, H.C., Ma, Y.S., 1996. Geology of Qaidam Basin and Its Petroleum Prediction. Geological Publishing House, Beijing (in Chinese).

Imbrie, J., Berger, A., Boyle, E.A., Clemens, S.C., Duffy, A., Howard, W.R., Kukla, G., Kutzbach, J., Martinson, D.G., McIntyre, A., Mix, A.C., Molfino, B., Morley, J.J., Peterson, L.C., Pisias, N.G., Prell, W.L., Raymo, M.E., Shackleton, N.J., Toggweiler, J.R., 1993. On the structure and origin of major glaciation cycles. 2. The 100,000-year cycle. Paleoceanography 8, 699–735.

Kapp, P., Pelletier, J.D., Rohrmann, A., Heermance, R., Russell, J., Ding, L., 2011. Wind erosion in the Qaidam Basin, central Asia: implications for tectonics, paleoclimate, and the source of the Loess Plateau. GSA Today 21, 4–10.

Laskar, J., Robutel, P., Joutel, F., Gastineau, M., Correia, A.C.M., Levrard, B., 2004. A long term numerical solution for the insolation quantities of the Earth. Astronomy & Astrophysics 428, 261–285.

Li, Z.X., Yao, T.D., Tian, L.D., Yu, W.S., Guo, X.J., Wang, Y.Q., 2006. Variation of $\delta^{18}O$ in precipitation in annual timescale with moisture transport in Delingha region. Earth Science Frontiers 13, 330–334 (in Chinese).

Licht, A., van Cappelle, M., Abels, H.A., Ladant, J.B., Trabucho-Alexandre, J., France-Lanord, C., Donnadieu, Y., Vandenberghe, J., Rigaudier, T., Lecuyer, C., Terry Jr., D., Adriaens, R., Boura, A., Guo, Z., Soe, A.N., Quade, J., Dupont-Nivet, G., Jaeger, J.J., 2014. Asian monsoons in a Late Eocene greenhouse world. Nature 513, 501–506.

Lisiecki, L.E., Raymo, M.E., 2005. A Pliocene–Pleistocene stack of 57 globally distributed benthic $\delta^{18}O$ records. Paleoceanography 20, PA1003. http://dx.doi.org/10.1029/2004PA001071.

Liu, X.D., Dong, B.W., 2013. Influence of the Tibetan Plateau uplift on the Asian monsoon–arid environment evolution. Chinese Science Bulletin 58, 4277–4291.

Liu, D.L., Fang, X.M., Song, C.H., Dai, S., Zhang, T., Zhang, W.L., Miao, Y.F., Liu, Y.Q., Wang, J.Y., 2010. Stratigraphic and paleomagnetic evidence of mid-Pleistocene rapid deformation and uplift of the NE Tibetan Plateau. Tectonophysics 486, 108–119.

Lu, Y., Fang, X.M., Appel, E., Wang, J.Y., Herb, C., Han, W.X., Wu, F.L., Song, C.H., 2015. 7.3–1.6 Ma grain size record of interaction between anticline uplift and climate change in the western Qaidam Basin, NE Tibetan Plateau. Sedimentary Geology 319, 40–51.

Maussion, F., Scherer, D., Mölg, T., Collier, E., Curio, J., Finkelnburg, R., 2014. Precipitation seasonality and variability over the Tibetan Plateau as resolved by the High Asia Reanalysis. Journal of Climate 27, 1910–1927.

Mölg, T., Maussion, F., Scherer, D., 2014. Mid-latitude westerlies as a driver of glacier variability in monsoonal High Asia. Nature Climate Change 4, 68–73.

Molnar, P., Boos, W.R., Battisti, D.S., 2010. Orographic controls on climate and paleoclimate of Asia: thermal and mechanical roles for the Tibetan Plateau. Annual Review of Earth and Planetary Sciences 38, 77–102.

Nie, J.S., Song, Y.G., King, J.W., Zhang, R., Fang, X.M., 2013. Six million years of magnetic grain-size records reveal that temperature and precipitation were decoupled on the Chinese Loess Plateau during ~4.5–2.6 Ma. Quaternary Research 79, 465–470.

https://doi.org/10.1016/j.yqres.2015.09.009 Published online by Cambridge University Press

Pross, J., Klotz, S., Mosbrugger, V., 2000. Reconstructing palaeotemperatures for the Early and Middle Pleistocene using the mutual climatic range method based on plant fossils. Quaternary Science Reviews 19, 1785–1799.
Qiu, J., 2008. The third pole. Nature 454, 393–396.
Ramstein, G., Fluteau, F., Besse, J., Joussaume, S., 1997. Effect of orogeny, plate motion and land–sea distribution on Eurasian climate change over the past 30 million years. Nature 386, 788–795.
Roberts, A.P., Pike, C.R., Verosub, K.L., 2000. First-order reversal curve diagrams: a new tool for characterizing the magnetic properties of natural samples. Journal of Geophysical Research 105, 28461–28475.
Rowan, C.J., Roberts, A.P., 2006. Magnetite dissolution, diachronous greigite formation, and secondary magnetizations from pyrite oxidation: unravelling complex magnetizations in Neogene marine sediments from New Zealand. Earth and Planetary Science Letters 241, 119–137.
Rowley, D.B., Currie, B.S., 2006. Palaeo-altimetry of the Late Eocene to Miocene Lunpola basin, central Tibet. Nature 439, 677–681.
Ruddiman, W.F., Kutzbach, J.E., 1989. Forcing of Late Cenozoic Northern Hemisphere climate by plateau uplift in southern Asia and the American west. Journal of Geophysical Research 94, 18409–18427.
Schulz, M., Stattegger, K., 1997. SPECTRUM: spectral analysis of unevenly spaced paleoclimatic time series. Computers & Geosciences 23, 929–945.
Sidhu, P.S., 1988. Transformation of trace element-substituted maghemite to hematite. Clays and Clay Minerals 36, 31–38.
Song, C.H., Gao, D.L., Fang, X.M., Cui, Z.J., Li, J.J., Yang, S.L., Jin, H.B., Burbank, D., Kirschvink, J.L., 2005. Late Cenozoic high-resolution magnetostratigraphy in the Kunlun Pass Basin and its implications for the uplift of the northern Tibetan Plateau. Chinese Science Bulletin 50, 1912–1922.
Sun, Y.B., An, Z.S., Clemens, S.C., Bloemendal, J., Vandenberghe, J., 2010. Seven million years of wind and precipitation variability on the Chinese Loess Plateau. Earth and Planetary Science Letters 297, 525–535 (data file URL: ftp://ftp.ncdc.noaa.gov/pub/data/paleo/loess/china/sun2010lingtai.xls; data accessed: 2014-09-24).
Tang, Z.H., Ding, Z.L., White, P.D., Dong, X.X., Ji, J.L., Jiang, H.C., Luo, P., Wang, X., 2011. Late Cenozoic central Asian drying inferred from a palynological record from the northern Tian Shan. Earth and Planetary Science Letters 302, 439–447.
van Velzen, A.J., Dekkers, M.J., 1999. Low-temperature oxidation of magnetite in loess–paleosol sequences: a correction of rock magnetic parameters. Studia Geophysica et Geodaetica 43, 357–375.
Wang, B., 2006. The Asian Monsoon. Springer, Berlin.
Wang, J., Wang, Y.J., Liu, Z.C., Li, J.Q., Xi, P., 1999. Cenozoic environmental evolution of the Qaidam Basin and its implications for the uplift of the Tibetan Plateau and the drying of central Asia. Palaeogeography Palaeoclimatology Palaeoecology 152, 37–47.
Wang, J.Y., Fang, X.M., Appel, E., Song, C.H., 2012. Pliocene–Pleistocene climate change at the NE Tibetan Plateau deduced from lithofacies variation in the drill core SG-1, western Qaidam Basin, China. Journal of Sedimentary Research 82, 933–952.
Winklhofer, M., Zimanyi, G.T., 2006. Extracting the intrinsic switching field distribution in perpendicular media: a comparative analysis. Journal of Applied Physics 99. http://dx.doi.org/10.1063/1.2176598 (08E710).
Winklhofer, M., Dumas, R.K., Liu, K., 2008. Identifying reversible and irreversible magnetization changes in prototype patterned media using first- and second-order reversal curves. Journal of Applied Physics 103. http://dx.doi.org/10.1063/1.2837888 (07C518).
Wu, F.L., Fang, X.M., Herrmann, M., Mosbrugger, V., Miao, Y.F., 2011. Extended drought in the interior of Central Asia since the Pliocene reconstructed from sporopollen records. Global and Planetary Change 76, 16–21.
Xia, W.C., Zhang, N., Yuan, X.P., Fan, L.S., Zhang, B.S., 2001. Cenozoic Qaidam Basin, China: a stronger tectonic inversed, extensional rifted basin. AAPG Bulletin 85, 715–736.
Xiao, J.L., Porter, S.C., An, Z.S., Kumai, H., Yoshikawa, S., 1995. Grain size of quartz as an indicator of winter monsoon strength on the Loess Plateau of central China during the last 130,000 yr. Quaternary Research 43, 22–29.
Xu, G.B., Chen, T., Liu, X.H., An, W.L., Wang, W.Z., Yun, H.B., 2011. Potential linkages between the moisture variability in the northeastern Qaidam Basin, China, since 1800 and the East Asian summer monsoon as reflected by tree ring $\delta^{18}O$. Journal of Geophysical Research 116, D09111. http://dx.doi.org/10.1029/2010JD015053.
Yang, Y.B., Fang, X.M., Appel, E., Galy, A., Li, M.H., Zhang, W.L., 2013a. Late Pliocene–Quaternary evolution of redox conditions in the western Qaidam paleolake (NE Tibetan Plateau) deduced from Mn geochemistry in the drilling core SG-1. Quaternary Research 80, 586–595.
Yang, Y.B., Fang, X.M., Galy, A., Appel, E., Li, M.H., 2013b. Quaternary paleolake nutrient evolution and climatic change in the western Qaidam Basin deduced from phosphorus geochemistry record of deep drilling core SG-1. Quaternary International 313–314, 156–167.
Yang, Y.B., Fang, X.M., Galy, A., Li, M.H., Appel, E., Liu, X.M., 2014. Paleoclimatic significance of rare earth element record of the calcareous lacustrine sediments from a long core (SG-1) in the western Qaidam Basin, NE Tibetan Plateau. Journal of Geochemical Exploration 145, 223–232.
Yang, Y.B., Fang, X.M., Li, M.H., Galy, A., Koutsodendris, A., Zhang, W.L., 2015. Paleoenvironmental implications of uranium concentrations in lacustrine calcareous clastic-evaporite deposits in the western Qaidam Basin. Palaeogeography Palaeoclimatology Palaeoecology 417, 422–431.
Yao, T.D., Thompson, L., Yang, W., Yu, W.S., Gao, Y., Guo, X.J., Yang, X.X., Duan, K.Q., Zhao, H.B., Xu, B.Q., Pu, J.C., Lu, A.X., Xiang, Y., Kattel, D.B., Joswiak, D., 2012. Different glacier status with atmospheric circulations in Tibetan Plateau and surroundings. Nature Climate Change 2, 663–667.
Yin, A., Dang, Y.Q., Zhang, M., McRivette, M.W., Burgess, W.P., Chen, X.H., 2007. Cenozoic tectonic evolution of Qaidam Basin and its surrounding regions (part 2): wedge tectonics in southern Qaidam basin and the Eastern Kunlun Range. Geological Society of America Special Papers 433, 369–390.
Yin, A., Dang, Y.-Q., Zhang, M., Chen, X.-H., McRivette, M.W., 2008. Cenozoic tectonic evolution of the Qaidam Basin and its surrounding regions (part 3): structural geology, sedimentation, and regional tectonic reconstruction. GSA Bulletin 120, 847–876.
Zachos, J., Pagani, M., Sloan, L., Thomas, E., Billups, K., 2001. Trends, rhythms, and aberrations in global climate 65 Ma to present. Science 292, 686–693.
Zhang, Y.G., Ji, J.F., Balsam, W.L., Liu, L.W., Chen, J., 2007. High resolution hematite and goethite records from ODP 1143, South China Sea: co-evolution of monsoonal precipitation and El Niño over the past 600,000 years. Earth and Planetary Science Letters 264, 136–150.
Zhang, Y.G., Ji, J.F., Balsam, W., Liu, L.W., Chen, J., 2009. Mid-Pliocene Asian monsoon intensification and the onset of Northern Hemisphere glaciation. Geology 37, 599–602.
Zhang, S.R., Xu, Q.H., Nielsen, A.B., Chen, H., Li, Y.C., Li, M.Y., Hun, L.Y., Li, J.Y., 2012a. Pollen assemblages and their environmental implications in the Qaidam Basin, NW China. Boreas 41, 602–613.
Zhang, W.L., Appel, E., Fang, X.M., Song, C.H., Cirpka, O., 2012b. Magnetostratigraphy of deep drilling core SG-1 in the western Qaidam Basin (NE Tibetan Plateau) and its tectonic implications. Quaternary Research 78, 139–148.
Zhang, W.L., Appel, E., Fang, X.M., Yan, M.D., Song, C.H., Cao, L.W., 2012c. Paleoclimatic implications of magnetic susceptibility in Late Pliocene–Quaternary sediments from deep drilling core SG-1 in the western Qaidam Basin (NE Tibetan Plateau). Journal of Geophysical Research 117, B06101. http://dx.doi.org/10.1029/2011JB008949.
Zhang, W.L., Fang, X.M., Song, C.H., Appel, E., Yan, M.D., Wang, Y.D., 2013. Late Neogene magnetostratigraphy in the western Qaidam Basin (NE Tibetan Plateau) and its constraints on active tectonic uplift and progressive evolution of growth strata. Tectonophysics 599, 107–116.
Zhang, W.L., Appel, E., Fang, X.M., Song, C.H., Setzer, F., Herb, C., Yan, M.D., 2014. Magnetostratigraphy of drill-core SG-1b in the western Qaidam Basin (NE Tibetan Plateau) and tectonic implications. Geophysical Journal International 197, 90–118.
Zhao, Y., Herzschuh, U., 2009. Modern pollen representation of source vegetation in the Qaidam Basin and surrounding mountains, north-eastern Tibetan Plateau. Vegetation History and Archaeobotany 18, 245–260.
Zhao, Y., Yu, Z.C., Chen, F.H., Ito, E., Zhao, C., 2007. Holocene vegetation and climate history at Hurleg Lake in the Qaidam Basin, northwest China. Review of Palaeobotany and Palynology 145, 275–288.
Zhao, Y., Liu, H.Y., Li, F.R., Huang, X.Z., Sun, J.H., Zhao, W.W., Herzschuh, U., Tang, Y., 2012. Application and limitations of the *Artemisia*/Chenopodiaceae pollen ratio in arid and semi-arid China. The Holocene 22, 1385–1392.

https://doi.org/10.1016/j.yqres.2015.09.009 Published online by Cambridge University Press